Research Article

Yu Liu, Heliang Wang, Xiwei Guo, Mingyuan Yi, Lihong Wan, Shuangquan Liao, Zhifen Wang*, and Lin Fang*

Xanthate-modified nanoTiO_2 as a novel vulcanization accelerator enhancing mechanical and antibacterial properties of natural rubber

https://doi.org/10.1515/ntrev-2021-0038
received May 14, 2021; accepted May 28, 2021

Abstract: With the emerging of sustainability, the fabrication of effective and eco-friendly agents for rubber industry has attracted extensive attention. In this study, a novel and nontoxic titanium dioxide-based vulcanization accelerator (xanthate-modified nanotitanium dioxide (TDSX)) with excellent antibacterial performance, for the first time, was synthesized under the catalyst of ceric ammonium nitrate. Notably, the thermal stability of xanthate was greatly enhanced after being grafted on titanium dioxide (TiO_2) nanoparticles, in which the activation energy was increased from 6.4 to 92.5 kJ/mol, enabling the obtained TDSX with multiple functions, mainly consisting of fabulous vulcanization-promoting effects, reinforcing effects, antibacterial properties, and anti-ultraviolet aging effects for natural rubber (NR). Simultaneously, the TDSX can be effectively and uniformly dispersed in the rubber matrix along with the developed interface interaction between TDSX particles and rubber matrix. Compared to the traditional accelerators 2-mercaptobenzothiazole (M) system, the tensile strength and the tearing strength of NR/TDSX was improved by 26.3 and 40.4%, respectively. Potentially, our work for preparing green vulcanization accelerator can provide a new design strategy for multifunctional high performance elastomer materials.

Keywords: nano titanium dioxide, vulcanization accelerator, natural rubber, antibacterial properties

1 Introduction

As one of the most strategically important elastic materials, natural rubber displays multitude of applications due to its remarkable properties, especially for outstanding malleability, high strength, and excellent resilience. However, currently, commercial small-molecule vulcanization accelerators generally face the issues of poor thermal stability, weak dispersion, and serious aggregation, finally leading to the environmental problems and unsatisfactory properties of the products [1]. Therefore, nowadays, numerous attempts have been taken to solve the aforementioned shortcomings, where the physical or chemical loading of small molecule additives onto inorganic fillers can be an effective approach to address the related issues [2]. Besides, with the development of sustainability, another typical problem for current vulcanization accelerators is the toxicity since they can generate nitrosamine compounds, which are believed to have a negative effect on the health of human. Thus, the preparation of nontoxic, environmentally friendly, high-performance vulcanization accelerators is rather essential in the rubber industry.

Vulcanization accelerator refers to the substance that can increase the vulcanization speed and lower the vulcanization temperature after adding the rubber compound. Xanthates are generally prepared from the reaction of sodium or potassium hydroxide with an alcohol and carbon disulfide, whose structural formula is R–O–C = S(S)–M (R represents alkyl groups and M represents metal atoms) [3]. Xanthate, an environmentally friendly and efficient vulcanization accelerator, has attracted

* **Corresponding author: Zhifen Wang,** College of Materials Science and Engineering, Hainan University, Haikou 570228, China, e-mail: wangzhifen2005@163.com, tel: +86-0898-66251982, fax: +86-0898-66279219
* **Corresponding author: Lin Fang,** College of Materials Science and Engineering, Hainan University, Haikou 570228, China, e-mail: fanglin206@163.com
Yu Liu, Heliang Wang, Mingyuan Yi, Lihong Wan, Shuangquan Liao: College of Materials Science and Engineering, Hainan University, Haikou 570228, China
Xiwei Guo: School of Science and Engineering, The Chinese University of Hong Kong, Shenzhen 518172, China

much attention in the latex industry since it does not generate carcinogens during processing [4]. Lamentedly, it remains a challenge for xanthate to be applied in the rubber industry due to serious self-aggregation and instability to temperature [5]. Therefore, a favorable method to deal with the aforementioned issues is to load xanthate on the filler [6]. For instance, Li *et al.* [7] used an eco-friendly starch as the carrier for xanthate to decline related drawback.

Natural rubber contamination by bacteria takes place easily that can affect both the quality and the price. Thus, Mourad *et al.* [8] investigated the incorporation of the prepared Ag-SiO_2 core shell particles in natural rubber matrix and the antibacterial properties of resulting composites. Thus, Xu *et al.* [9] prepared a functional TiO_2/Ser (sericite) composite to improve the antibacterial properties of rubber products, such as medical carriers and food packaging.

Due to significant difference in size compared to their bulk materials, TiO_2 nanoparticles have attracted much attention for their high surface-to-volume ratio and adaptability for multiple functions. It is a promising carrier, which can be widely used in rubber composites owing to low cost, absence of toxicity, and fabulous antimicrobial performance [10]. Unfortunately, due to the poor compatibility and serious self-aggregation caused by extremely small size and the hydroxyl on the surface of TiO_2 nanoparticles [11], it is still difficult for TiO_2 nanoparticles to be uniformly dispersed in the rubber matrix. To address these issues, various strategies have been employed to functionalize the surface of TiO_2 nanoparticles for reducing undesirable interactions and favoring desired interactions [12]. Herein, we selected cerium ammonium nitrate, a powerful oxidant [13], to address relevant problems since cerium ammonium nitrate work similar to the Lewis acid catalyst and has powerful oxidation capacity.

To the best of our knowledge, there is no reported study on the preparation of TiO_2 nanoparticle-grafted xanthate vulcanization accelerator, where cerium ammonium nitrate worked as a catalyst. In detail, to solve the problem of xanthate migration and self-assembly of TiO_2 nanoparticles, cerium ammonium nitrate worked as the oxidizing agent of the hydroxyl groups of TiO_2 nanoparticles to improve the reactivity of hydroxyl, ultimately achieving the successful preparation of chemically grafted xanthate on TiO_2 nanoparticles (TDSX). A comparative study on the antibacterial performances and mechanical and thermal properties of NR/TDSX, NR/M, and NR/(M/TDSX) composites was also carried out. We believe that our study can provide a new approach to fabricate multifunctional vulcanization accelerators with antibacterial properties by simple catalysis of high valence metal ions, which is expected to expand the application range of natural rubber.

2 Experimental section

2.1 Materials

Natural rubber (SCR4) was afforded by JinShui processing plant of Hainan Rubber Group. Ceric ammonium nitrate, carbon disulfide (CS_2), and TiO_2 were provided from Shanghai Aladdin Bio-Chem Technology Co., Ltd. The surface area and the moisture content of TiO_2 nanoparticles were 2.3×10^6 m^2/g and 1.5 wt%, respectively. Sodium hydroxide (NaOH) and *N*,*N*-dimethylformamide were offered from Guangzhou Chemical Reagent Company. Sodium isobutyl xanthate was afforded by Qixia Aotong Chemical Co., Ltd., China. Zinc oxide (ZnO), sulfur (S), stearic acid (SA), and 2-mercapto-benzothiazole (M) were of industrial grade.

2.2 Synthesis of TDSX accelerator

TiO_2 nanoparticles was dried in an air-dry oven at 80°C for 1 h. Then, 26 g dried titanium dioxide and 650 mL *N*,*N*-dimethylformamide were added in a three-necked flask successively. The mixture was stirred with 3.5 g ceric ammonium nitrate at 80°C for 2 h to activate hydroxyl groups on the surface of TiO_2 nanoparticles. Thereafter, 40 g solid NaOH was added in the three-necked flask at 35°C for 1 h under continuous stirring, followed by 76 g CS_2 that was slowly dripped inside. To obtain the TDSX vulcanization accelerator, the mixture was stirred for 3 h, filtered, and dried under reduced pressure at 40°C for 36 h. The synthesis route of TDSX is show in Figure 1.

2.3 Preparation of natural rubber composites

The formulas of natural rubber composites were carried out as presented in Table 1. In the investigation of the optimal proportion of TDSX, TDSX was used as a vulcanization accelerator at loadings of 4, 5, 6, 7, and 8 parts per hundred parts of rubber (phr). Then, the natural rubber composites containing the best ratio of TDSX and the M (fixed at 0.7 phr) curing system were compared.

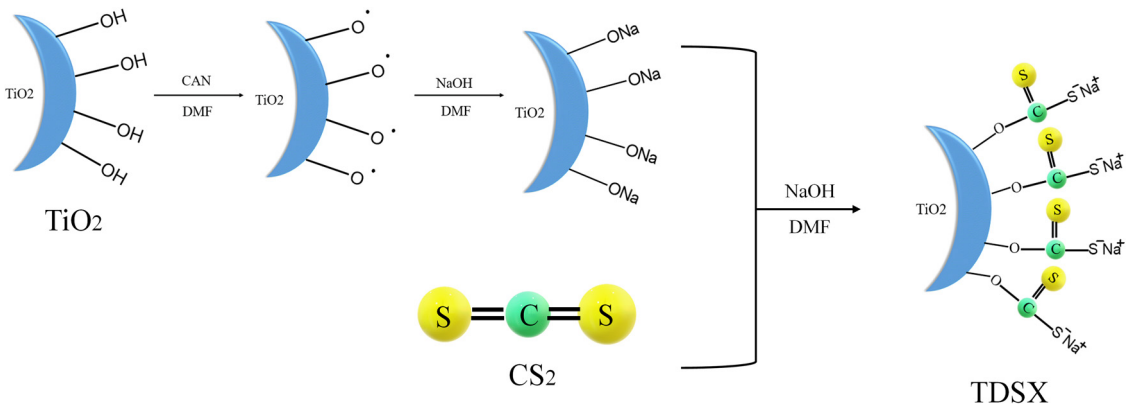

Figure 1: The synthetic route of TDSX.

Table 1: Formulas of NR/TDSX, NR/M and NR/(M/TiO_2)

Sample series	Component (phr)						
	NR	TiO_2	TDSX[a]	M	SA	ZnO	S
NR/TDSX-4 phr	100	0	4	0	2	6	3.5
NR/TDSX-5 phr	100	0	5	0	2	6	3.5
NR/TDSX-6 phr	100	0	6	0	2	6	3.5
NR/TDSX-7 phr	100	0	7	0	2	6	3.5
NR/TDSX-8 phr	100	0	8	0	2	6	3.5
NR/M[b]	100	0	0	0.7	2	6	3.5
NR/(M/TiO_2)[c]	100	6.3	0	0.7	2	6	3.5

[a]The content of TDSX for composites was 4, 5, 6, 7, and 8 phr, respectively. [b]The dosage of M was calculated according to the effective component of xanthate and the grafting efficiency of TDSX (9.6 wt%). TiO_2 is not added to NR/M. [c]The ingredients of NR/(M/TiO_2) was equivalent to NR/TDSX-7 phr composites.

Natural rubber and other additives were successively compounded with samples on a two-roll mill within 12 min. After homogenization, the composites were subjected to compression at 145°C for the optimum curing time (T90) to generate sulfur crosslinks [14].

2.4 Characterization

Fourier transform infrared (FTIR) spectroscopy of untreated TiO_2 and TDSX recorded on a PerkinElmer spectrometer with the highly pure potassium bromide tableting was performed. X-ray photoelectron spectroscopy (XPS) was carried out on an Axis Supra with an aluminum (mono) Kα source (1486.6 eV). Carbon-13 nuclear magnetic resonance (^{13}C-NMR) (600 MHz JNM- ECZ600R spectrometer, JEOL, Japan) was used to elucidate the chemical structure of the material. To determine the hydrophobicity of TDSX and TiO_2, the static contact angle of a droplet on the surface was measured and analyzed by a Kruss DSA 30 (Germany) contact angle goniometer [15]. The thermogravimetric analysis (TGA) was performed using a Mettler-Toledo TGA/DSC subjected to a heating rate of 10°C/min in a heating range of 25–500°C, in which the activation energies (E_a) of thermal degradation in the main degradation stage were calculated according to the following equations [16]:

$$\alpha = \frac{w_0 - w_t}{w_0 - w_\infty}, \tag{2.1}$$

$$\ln\left[\ln\left(\frac{1}{1-\alpha}\right)\right] = -\frac{E_a}{RT} + \ln\left[\left(\frac{R}{E_a}\right)\left(\frac{A}{\beta}\right)T^2 m\right], \tag{2.2}$$

where W_0, W_t, and W_∞ are the mass of samples at the initial time, mass at a given time, and final sample weight, respectively. α is the degradation rate, R is the gas constant (8.314 J/mol/K), and T is the absolute temperature (K).

The bonding rubber content on the surface of TDSX particles and TiO_2 particles was calculated according to the means suggested in the study by Ahn *et al.* [17]. The curves of vulcanization were obtained by rotorless rheometer MOR-2000E (Electronics Wuxi Liyuan Chemical Equipment Co., Ltd) at 145°C [18]. Mechanical properties were analyzed using an electronic universal testing machine (WDW-0.5C) provided by Hualong Test Instruments Corporation, Shanghai. The surface and the morphology of tensile fracture were analyzed by a Phenom prox scanning electron microscope (SEM). The abrasion was determined by previously reported methods [19].

To characterize the ability of molecular chains motion, dynamic mechanical analysis (DMA) was performed by a TA DMA Q850 instrument in a tensile mode at a frequency of 5 Hz and a heating rate of 3°C/min [20]. Crosslinking density of vulcanized natural rubber composites was determined by the equilibrium swelling method in toluene and

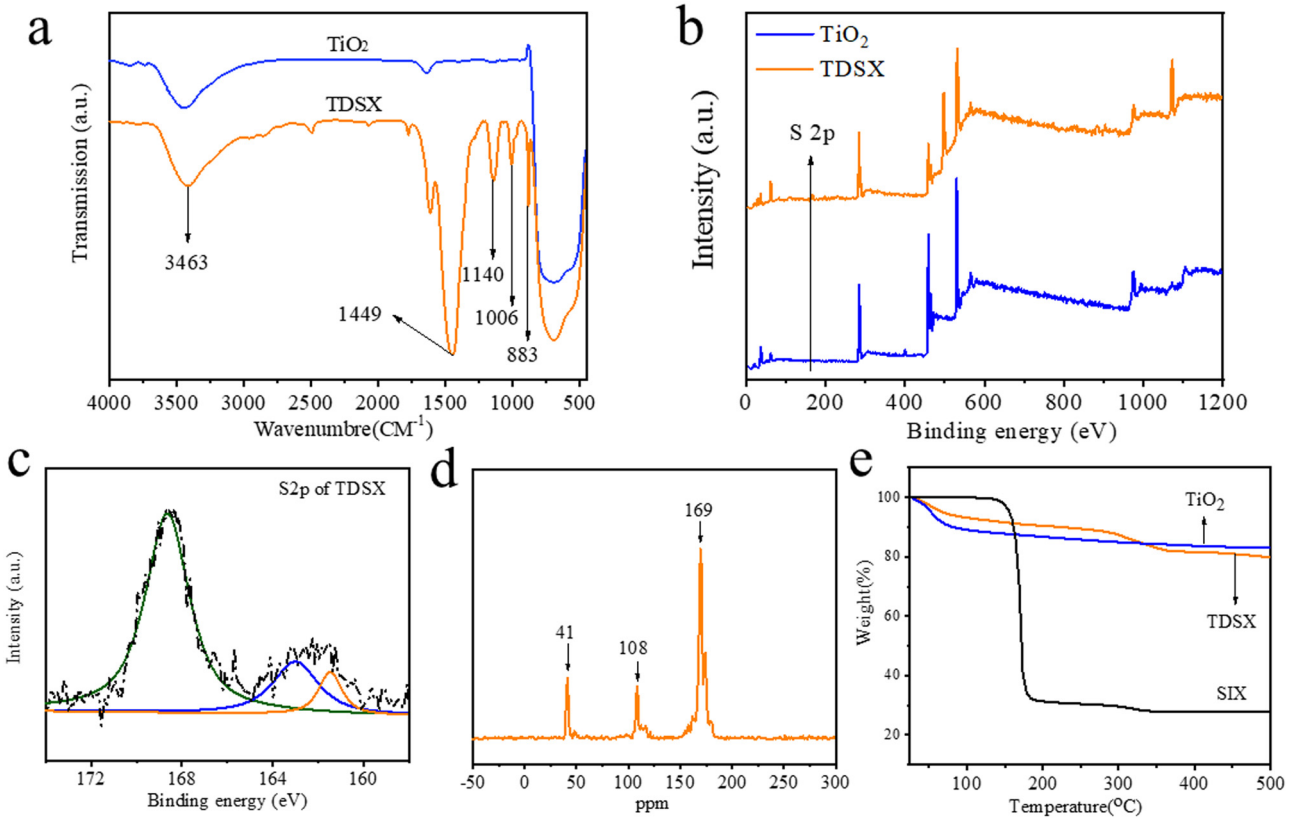

Figure 2: (a) FTIR spectra of TiO_2 nanoparticles and TDSX; (b) XPS spectra of TiO_2 nanoparticles and TDSX; (c) the high-resolution XPS spectra of TDSX; (d) ^{13}C MAS NMR spectra; (e) TG curves of TiO_2 nanoparticles and TDSX and sodium isobutyl xanthate.

Table 2: The characteristic parameters (initial temperature (T_0), final temperature (T_f), temperature at maximum decomposition rate (T_p), and E_a) of thermal degradation of sodium isobutyl xanthate and TDSX

Sample	T_0 (°C)	T_p (°C)	T_f (°C)	E_a (kJ/mol)
Sodium isobutyl xanthate	151.8	168.9	194.1	6.43
NanoTiO$_2$ grafted the xanthate	204.9	321.4	398.5	92.5

was calculated according to the classical Flory–Rehner equation [21].

The antibacterial activity was investigated against *Escherichia coli* (A TCC 25922, Gram-negative) and *Staphylococcus aureus* (CMCC(B) 26003, Gram-positive) using the flat colony counting method [22]. The sterilized NR/M, NR/TiO_2, and NR/TDSX samples were placed in the *E. coli* and *S. aureus* liquid culture medium for 24 h, and then 50 µL of the liquid bacterial culture medium was taken from each, diluted, and evenly dispersed with a coating rod on nutrient agar. The number of viable bacteria after 24 h of cultivation was calculated to investigate its antibacterial properties [23]. The vulcanized rubber was cut into dumbbell-shaped specimens and placed in the UV aging test box. Aging at a temperature of 50°C for 8 days, the radiation intensity is 0.8 W/m^2 [24].

3 Results and discussion

To figure out the success of reaction and loading efficiency, FTIR, XPS, ^{13}C-NMR, and TGA were subsequently used to check out the changes. Figure 2(a) shows the FTIR spectrum of TiO_2 nanoparticles and TDSX.

The peak at 3,428 cm^{-1} is the stretching vibration absorption peak of the hydroxyl group (–OH) caused by water or adsorbed water. The strong band at 1,449 cm^{-1} corresponds to the characteristic band of the carbonyl group [25]. Compared to TiO_2, the newly generated peaks on TDSX at 1,006, 1,140, and 883 cm^{-1}, which were attributed to the absorptions of C–O, C═S, and C–S, respectively, indicated that sodium xanthate has been successfully *in situ* formed onto the surface of TiO_2 nanoparticles. Thereafter, the related chemical natures of the surface

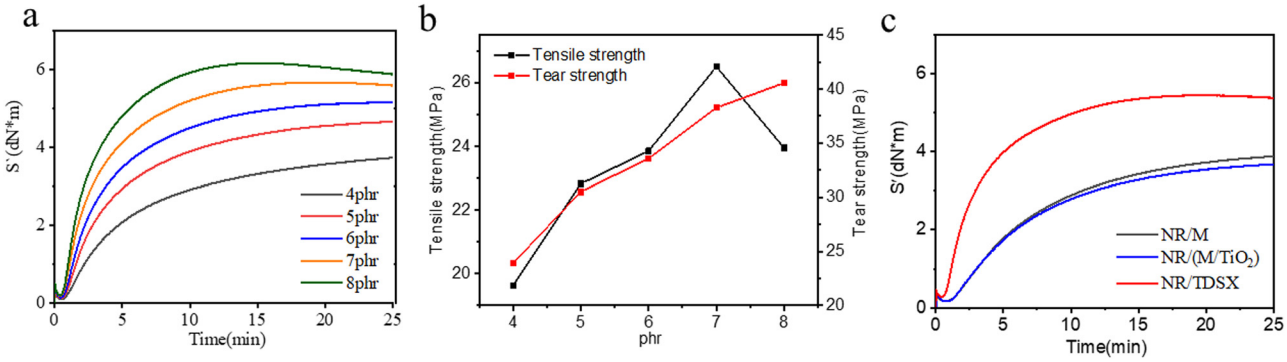

Figure 3: (a) The curing curve of natural rubber composites with different contents of TDSX; (b) the tensile strength and the tear strength of natural rubber composites with different contents of TDSX; and (c) the curing curve of NR/M, NR/(M/TiO_2), and NR/TDSX.

Table 3: The curing parameters of natural rubber compounds

Sample	T90 (min)	ML (dN m)	MH (dN m)	MH–ML (dN m)
NR/4 phr	20.63	0.10	3.98	3.88
NR/5 phr	14.27	0.13	4.74	4.61
NR/6 phr	11.47	0.14	5.17	5.03
NR/7 phr	9.42	0.19	5.68	5.49
NR/8 phr	7.73	0.20	6.18	5.98
NR/M	17.70	0.18	3.98	3.80
NR/(M/TiO_2)	16.97	0.17	3.76	3.59

species were the checked by XPS (Figure 2b). The newly induced peak at 168.2 eV corresponding to S 2p of TDSX was observed. The detailed spectrum of S element (Figure 2c) shows that the S 2p (161.4 and 163.3 eV), which belong to the existence of S element with two kinds of chemical structures [26], were presented in the spectrum of TDSX. The peak at 168.6 eV may be due to the existence of residual CS_2.

Besides, this information was further confirmed by the results of ^{13}C-NMR (Figure 2d). The signal at 169 ppm is assigned to the O–C(=S)–S in TDSX, while a weak signal at 108 and 41 ppm belonging to the signals of residual DMF solvent is observed. All of the results demonstrate that TDSX has been successfully prepared. TGA was subsequently carried out to illustrate the loading efficiency and related thermal properties [27] (Figure 2e and Table 2). Compared to sodium isobutyl xanthate, the values of T_0, T_p, and T_f for TDSX were as expected increased by 53.1, 152.5, and 204.4°C respectively, which were in well accordance with the change of E_a since it was dramatically enhanced from 6.4 to 92.5 kJ/mol, suggesting that the thermal stability of xanthate was significantly improved. In addition, according to the weight losses of titanium dioxide and TDSX in the temperature region between 200 and 500°C, the grafting efficiency of TDSX was 9.6 wt%.

Subsequently, a systematic comparison of vulcanization behaviors and mechanical properties for various samples was done (Figure 3a–c and Table 3). T90 is the optimum vulcanization time, and its decrease indicates that the vulcanization speed is accelerated. The difference between minimum torque and maximum torque (MH–ML) characterizes the degree of vulcanization of the rubber [28]. Obviously, the cross-linking process at 145°C shows a significant discrepancy (Figure 3(a)). Although 8 phr of TDSX have a lower T90 and higher MH–ML, it is considered that the flat vulcanization period is conducive to the industrialization of rubber [29], and the best content of TDSX was 7 phr. Figure 3(b) shows the changes in the tensile strength and tear strength with the addition of TDSX. The tear strength increased with the amount of TDSX. The tensile strength increased with the content of TDSX, where the tensile strength reached the maximum at the TDSX content of 7 phr, valuing at 26.88 MPa. When the content of TDSX was increased to 8 phr, the tensile strength, however, decreases to 23.94 MPa. The following sections were conducted based on the 7 phr. Notably, compared with the systems of M and M/TiO_2, the TDSX enabled enhancement of the elevated values of MH–ML and declining in T90 (Figure 3c).

Since dispersion of filler plays a vital role in mechanical properties of natural rubber products, SEM was then used to check the fracture surfaces of various systems [30] (Figure 4a).

The rubber molecular chains adsorbed on the surface of the nanoparticles appear to slip and straighten orientation during the stretching process, which can effectively enhance the degree of orientation and strengthen

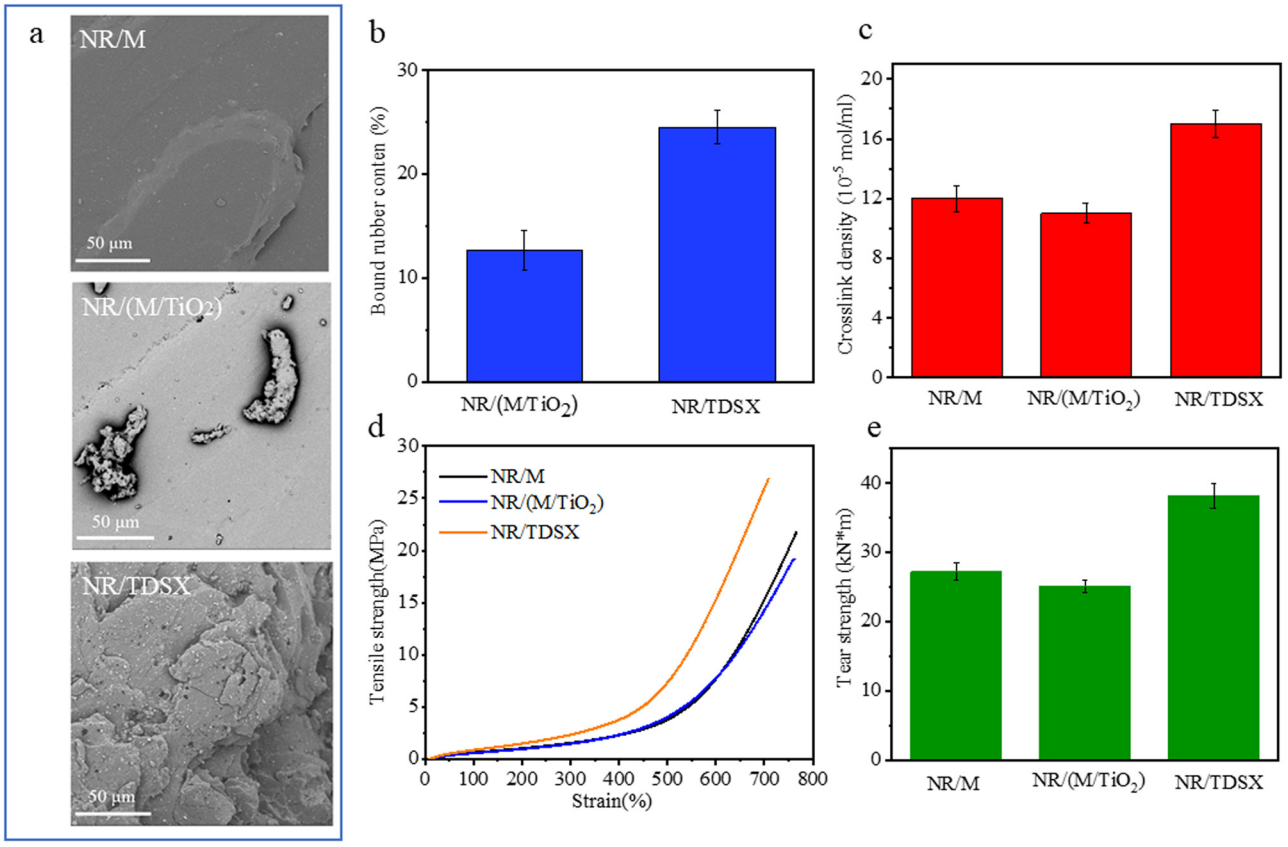

Figure 4: (a) SEM images for various samples; (b) the bound rubber content; (c) crosslink density; (d) curves of stress–strain; and (e) tear strength.

the rubber matrix [31]. The surface of NR/M was smooth, and the tensile strength was low since there are no nanoparticles added to the NR/M. Besides, aggregated TiO_2 particles in large sizes are easily observed in NR/(M/TiO_2), illustrating that the dispersion of TiO_2 was not even due to the hydrophilicity caused by hydroxyl groups, while that for TDSX was excellent [32]. The aggregated particles in the rubber matrix are not conducive to the performance of the adsorption efficiency and are very negative to the reinforcing result [33]. Therefore, the tensile strength and the tear strength of NR/(M/TiO_2) were even worse than those of NR/M.

In addition, the blurry interface between TDSX and natural rubber also proved that the formation of xanthate on the surface of TiO_2 nanoparticles overcame an incompatibility between TiO_2 and rubber and improved interfacial adhesion among the two phases [34]. Besides, TDSX-based natural rubber composite displayed the relatively high bound rubber contents (Figure 4b), meaning more rubber chains are anchored on the surface of TDSX particles. It may be induced by the strong interaction between TDSX and rubber matrix during the vulcanization of rubber chains since TDSX particles could be homogenously dispersed to form enhanced contact area to rubber chains [35].

To quantify the degree of filler–rubber interactions in vulcanizates, equilibrium swelling measurement is used to obtain crosslinking density [36]. The existence of TDSX leads to maximal effective crosslinking density (Figure 4c), indicating NR/TDSX composite had a most mature cross-linked network [37]. In consequence, both filler network and filler–rubber interaction were enhanced in NR/TDSX. Benefiting from the excellent dispersion and enhanced interaction of TDSX as well as high crosslinking density, the obtained TDSX functionalized natural rubber composite acquired superior mechanical properties as shown in Figure 4d and e. The tensile strength of TDSX-filled natural rubber vulcanizates was increased by 23.6 and 39.1% while the tear strength of NR/TDSX also simultaneously showed an increase by 40.4 and 52.2% compared to that of NR/M and NR/(M/TiO_2) containing equivalent components. Meanwhile, the TDSX enabled natural rubber with a relatively lower abrasion, valuing at 0.73 cm^{-3}/1.61 km, respectively (Figure 5a), illustrating the higher efficiency in suppressing tearing of NR/TDSX.

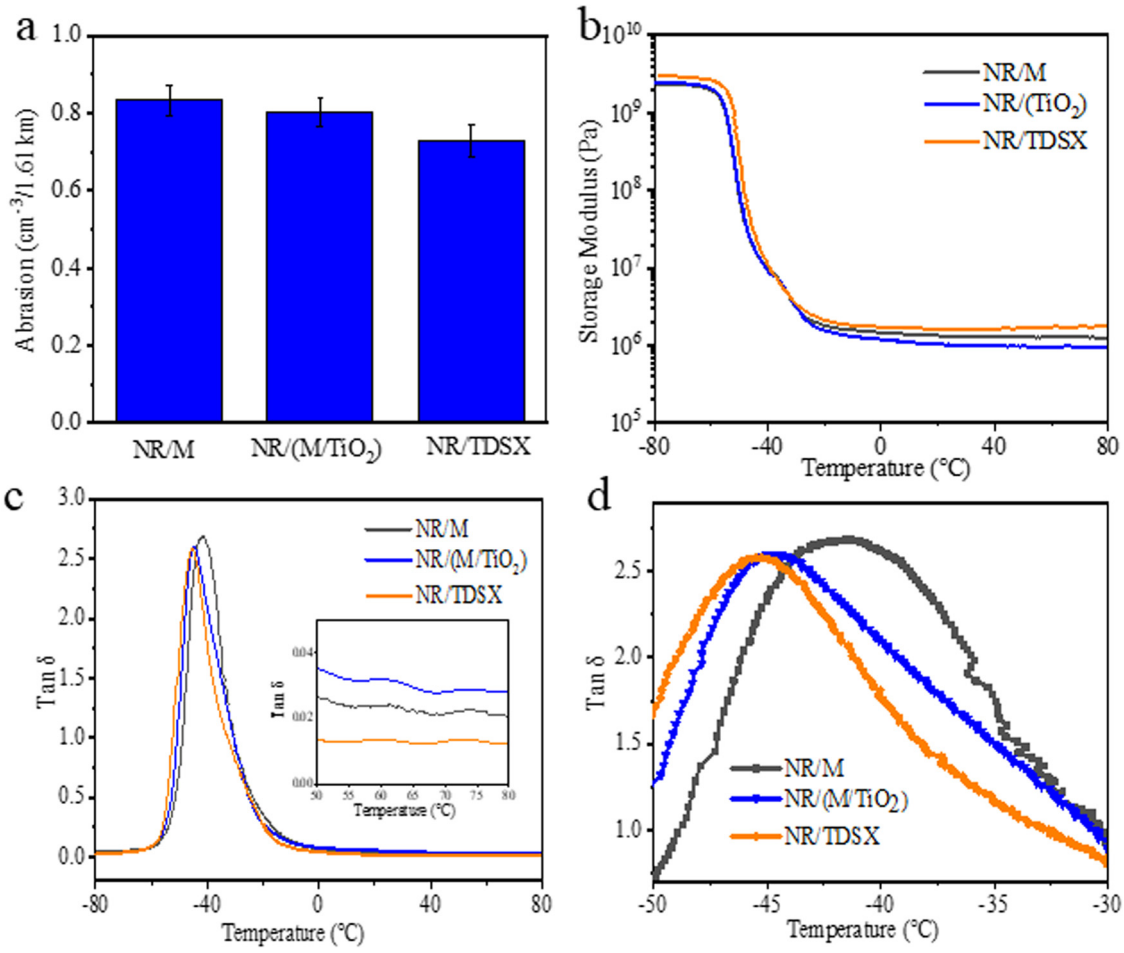

Figure 5: (a) abrasion of NR composites; (b) the storage modulus; (c) the tan δ curves; and (d) the high-definition tan δ curves.

Furthermore, the dynamic mechanical analysis (DMA) of NR/M and NR/(M/TiO_2) composites was conducted to investigate the related vulcanization effects (Figure 5b–d), which displayed variations of the storage modulus (E') and loss factor (tan δ) as a function of temperature [38]. Generally, a depression in tan δ height indicated the reduction number of mobile polymer chains during the glass transition, and the relative peak height is proportional to the volume of the constrained polymer chains [39]. The peak height of tan δ for NR/TDSX composite further decreased compared to that of NR/M and NR/(M/TiO_2) composites, meaning that more rubber chains were constrained in TDSX than those in M and M/TiO_2. This is in well agreement with the result of bound rubber content.

Besides, the NR/TDSX composite exhibited the highest value of E' (Figure 5b), which was probably due to the enhanced cross-linking density [40]. In addition, a lower tan δ 60°C value means a lower rolling resistance, which is an important parameter to evaluate the rolling resistance for high-performance rubber production [41]. It was obvious that the rolling resistance value of the NR/TDSX composites was the lowest as shown in Figure 5(d). Hence, the NR/TDSX composites exhibited remarkable improvements in their static and dynamic mechanical properties, suggesting that the NR/TDSX composites would be rather competitive in potential applications as green tire materials.

Ultimately, thanks to the existing and well dispersion of TiO_2 nanoparticles, the obtained NR/TDSX exhibited outstanding antibacterial behavior by inhibiting the growth of *Staphylococcus aureus* (Gram-positive) and *Escherichia coli* (Gram-negative) in contrast to that of NR/M and NR/(M/TiO_2) composites, which can be evaluated by the flat colony counting method [42] (Figure 6). The colonies of *S. aureus* and *E. coli* of both NR/M and NR/(M/TiO_2) vulcanizates are greater than 500, while NR/TDSX produces almost no colonies, demonstrating that the most efficient antibacterial specimen was NR/TDSX.

With the increase in UV aging time, the tensile strength of composites in the three systems all decreased

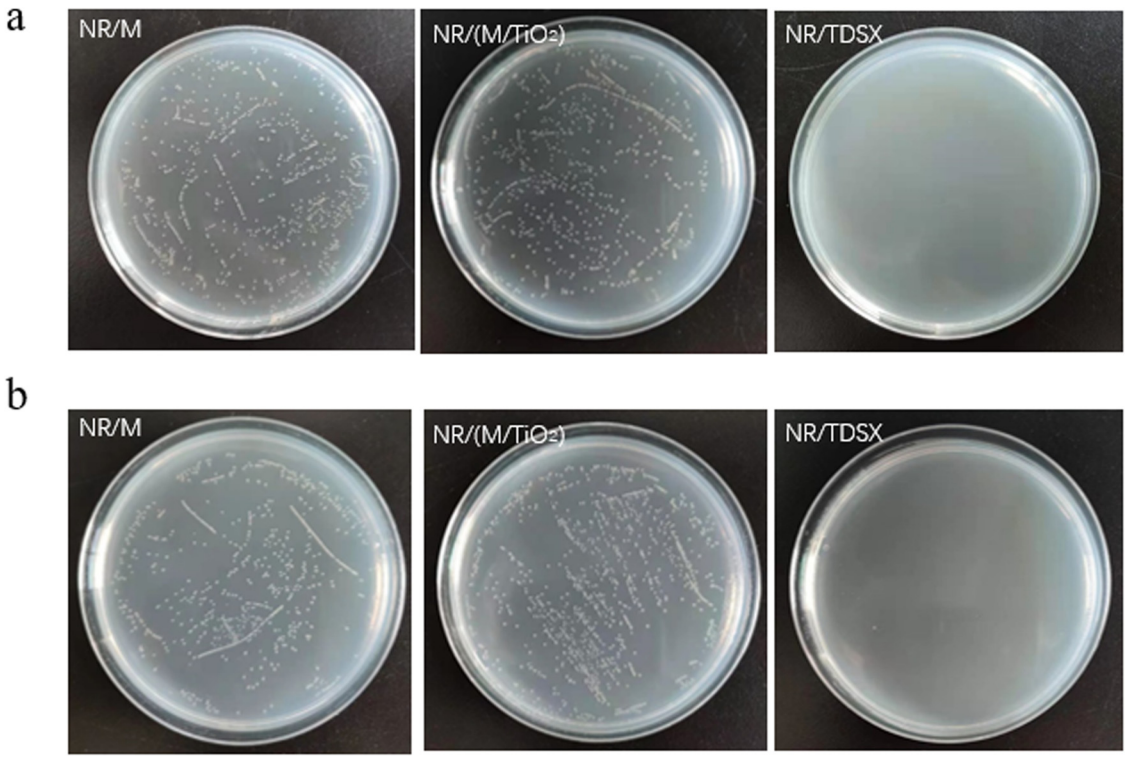

Figure 6: Antibacterial properties of NR composites against *Escherichia coli* (a) and *Staphylococcus aureus* (b).

to varying degrees (Figure 7a). After 8 days of UV aging, the tensile strength retention rates of NR/M, NR/(M/TiO$_2$), and NR/TDSX were 60.7, 64.9, and 85.1%, respectively. Meanwhile, the elongation at break of the NR/M and NR/(M/TiO$_2$) decreased to 80.9 and 82.1% of their original states (Figure 7b), respectively, while that for the NR/TDSX composite was barely affected under the UV aging, indicating that TDSX can improve the anti-ultraviolet aging performance of natural rubber and resist the damage of mechanical properties caused by ultraviolet aging.

4 Conclusion

In summary, a successful synthesis of a multifunctional vulcanization accelerator through an *in situ* method by

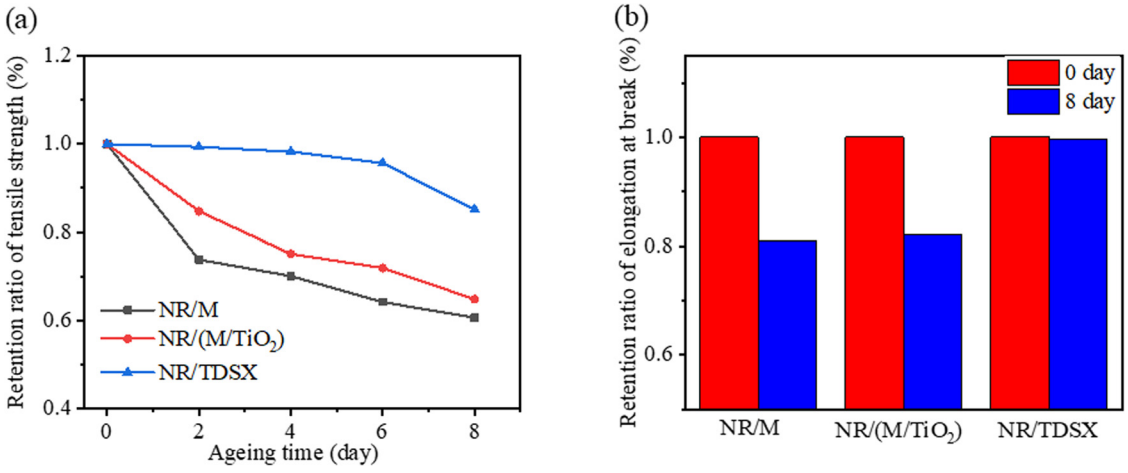

Figure 7: (a) The retention of tensile strength of different vulcanization systems and (b) the retention of elongation at break after 8 days of aging.

the reaction between CS_2 and TiO_2 nanoparticles under the catalyst of ceric ammonium nitrate, was achieved. The enhanced thermal degradation of (TDSX) enabled it to be used as an efficient vulcanization accelerator for rubber at normal vulcanization temperature (145°C). Besides, TDSX can evenly be dispersed in the natural rubber matrix owing to the strong interface interaction among TDSX and natural rubber (NR) matrix. In addition, the NR/TDSX with enhanced mechanical properties showed good antibacterial effect and anti-ultraviolet aging capability. It is believed that new methods to fabricate eco-friendly and multifunctional vulcanization accelerator may open up new horizons for the development of the rubber industry.

Funding information: The authors are grateful for the financial supports by High-Level Talent Program of Hainan Province (2019RC140) and the National Natural Science Foundation of China (51663008).

Author contributions: All authors have accepted responsibility for the entire content of this manuscript and approved its submission.

Conflict of interest: The authors state no conflict of interest.

References

[1] Cheng C, Song WH, Zhao Q, Zhang HL. Halloysite nanotubes in polymer science: purification, characterization, modification and applications. Nanotechnol Rev. 2020;9(1):323–44.
[2] Zhong B, Jia Z, Hu D, Luo Y, Jia D, Liu F. Enhancing interfacial interaction and mechanical properties of styrene-butadiene rubber composites via silica-supported vulcanization accelerator. Compos Part A Appl Sci Manuf. 2017;96:129–36.
[3] Lopez-Lopez EE, Lopez-Jimenez SJ, Barroso-Flores J, Rodriguez-Cardenas E, Tapia-Tapia M, Lopez-Tellez G, et al. Electrochemical reactivity of S-phenacyl-O-ethyl-xanthates in hydroalcoholic (MeOH/H_2O 4:1) and anhydrous acetonitrile media. Electrochim Acta. 2021;380:1–14.
[4] Sivaselvi K, Varma VS, Harikumar A, Jayaprakash A, Sankar S, Krishna CY, et al. Improving the mechanical properties of natural rubber composite with carbon black (N220) as filler. Mater Today: Proc. 2021;42:921–5.
[5] Kalgotra N, Andotra S, Kumar S, Gupta B, Pandey SK. Synthesis spectral, electrochemical, thermal and biological studies of benzyl/tolylxanthates of cadmium(II). J Indian Chem Soc. 2017;94(8):839–56.
[6] Zhu KZ, Liu Y, Wang HL, Guo XW, Liao SQ, Wang ZF, et al. Xanthate-modified silica as a novel multifunctional additive for properties improvement of natural rubber. Compos Sci Technol. 2021;203:1–8.
[7] Li KC, You JH, Liu Y, Zhu KZ, Xue CL, Guo XW, et al. Functionalized starch as a novel eco-friendly vulcanization accelerator enhancing mechanical properties of natural rubber. Carbohydr Polym. 2020;231:1–9.
[8] Mourad RM, Darwesh OM, Abdel-Hakim A. Enhancing physico-mechanical and antibacterial properties of natural rubber using synthesized Ag-SiO_2 nanoparticles. Int J Biol Macromol. 2020;164:3243–9.
[9] Xu Y, Feng L, Cong H, Li P, Liu F, Song S, et al. Preparation of TiO_2/Ser filler with ultraviolet resistance and antibacterial effects and its application in SBR/TRR blend rubber. J Rubber Res. 2020;23(2):47–55.
[10] Sun PP, Wang SZ, Li YH, Zhang T, Wang D, Zhang BQ, et al. One-pot synthesis of nano titanium dioxide in supercritical water. Nanotechnol Rev. 2020;9(1):410–7.
[11] Kong X, Yang D, Ni Y, Hao J, Guo W, Zhang L. Enhanced actuation strains of rubber composites by combined covalent and noncovalent modification of TiO_2 nanoparticles. Ind Eng Chem Res. 2019;58(43):19890–8.
[12] Kusworo TD, Ariyanti N, Utomo DP. Effect of nano-TiO_2 loading in polysulfone membranes on the removal of pollutant following natural-rubber wastewater treatment. J Water Process Eng. 2020;35:101190.
[13] Krylov IB, Paveliev SA, Matveeva OK, Terent'ev AO. Cerium(IV) ammonium nitrate: reagent for the versatile oxidative functionalization of styrenes using *N*-hydroxyphthalimide. Tetrahedron. 2019;75(17):2529–37.
[14] Zhang SY, Zhong RP, Hong RY, Hui D. On factors affecting surface free energy of carbon black for reinforcing rubber. Nanotechnol Rev. 2020;9(1):170–81.
[15] Maghsoudi K, Vazirinasab E, Momen G, Jafari R. Icephobicity and durability assessment of superhydrophobic surfaces: the role of surface roughness and the ice adhesion measurement technique. J Mater Process Technol. 2021;288:1–13.
[16] Wu J, Li K, Pan X, Liao S, You J, Zhu K, et al. Preparation and physical properties of porous starch/natural rubber composites. Starch-Starke. 2018;70:11–2.
[17] Ahn B, Kim D, Kim K, Kim IJ, Kim HJ, Kang CH, et al. Effect of the functional group of silanes on the modification of silica surface and the physical properties of solution styrene-butadiene rubber/silica composites. Compos Interfaces. 2019;26(7):585–96.
[18] Wei YC, Liu GX, Zhang L, Zhao FC, Liao SQ, Luo MC. Exploring the unique characteristics of natural rubber induced by coordination interaction between proteins and Zn^{2+}. Polymer. 2020;193:1–7.
[19] Dhanorkar RJ, Mohanty S, Gupta VK. Synthesis of functionalized styrene butadiene rubber and its applications in SBR-silica composites for high performance tire applications. Ind Eng Chem Res. 2021;60(12):4517–35.
[20] Yu WW, Xu WZ, Xia JH, Wei YC, Luo MC. Toughening natural rubber by the innate sacrificial network. Polymer. 2020;194:122419.
[21] Fu X, Xie ZT, Wei LY, Huang C, Luo MC, Huang GS. Detecting structural orientation in isoprene rubber/multiwall carbon nanotube nanocomposites at different scales during uniaxial deformation. Polym Int. 2018;67(3):258–68.
[22] Chen X, Wang ZF, Wu J. Processing and characterization of natural rubber/stearic acid-tetra-needle-like zinc oxide

whiskers medical antibacterial composites. J Polym Res. 2018;25(2):1–12.
[23] Dejen KD, Zereffa EA, Murthy HCA, Merga A. Synthesis of ZnO and ZnO/PVA nanocomposite using aqueous Moringa Oleifeira leaf extract template: antibacterial and electrochemical activities. Rev Adv Mater Sci. 2020;59(1):464–76.
[24] Wang L, Cui SC, Feng L. Research on the influence of ultraviolet aging on the interfacial cracking characteristics of warm mix crumb rubber modified asphalt mortar. Constr Build Mater. 2021;281:1–13.
[25] Zou Y, He J, Tang Z, Zhu L, Liu F. Structural and mechanical properties of styrene-butadiene rubber/silica composites with an interface modified in-situ using a novel hindered phenol antioxidant and its samarium complex. Compos Sci Technol. 2020;188:1–11.
[26] Makhlouf MM, Radwan AS, Ghazal B. Experimental and DFT insights into molecular structure and optical properties of new chalcones as promising photosensitizers towards solar cell applications. Appl Surf Sci. 2018;452:337–51.
[27] Zhu K, Pan Y, Wu J, Li K, Zhang Y. Functionalized silica as an eco-friendly vulcanization accelerator to enhance the interfacial interaction in NR/silica composites. Rubber Chem Technol. 2020;94(1):200–12.
[28] Bayat H, Fasihi M, Zare Y, Rhee KY. An experimental study on one-step and two-step foaming of natural rubber/silica nanocomposites. Nanotechnol Rev. 2020;9(1):427–35.
[29] Dziemidkiewicz A, Anyszka R, Blume A, Maciejewska M. Reaction mechanism of halogenated rubber crosslinking using a novel environmentally friendly curing system. Polym Test. 2020;84:106354.
[30] Dong H, Jia Z, Chen Y, Luo Y, Zhong B, Jia D. One-pot method to reduce and functionalize graphene oxide via vulcanization accelerator for robust elastomer composites with high thermal conductivity. Compos Sci Technol. 2018;164:267–73.
[31] Bokobza L. Filled elastomers: a new approach based on measurements of chain orientation. Polymer. 2001;42(12):5415–23.
[32] Nakonieczny DS, Antonowicz M, Paszenda Z. Surface modification methods of ceramic filler in ceramic-carbon fibre composites for bioengineering applications – a systematic review. Rev Adv Mater Sci. 2020;59(1):586–605.
[33] Zhang LQ. Rubber nanocomposites: basics and applications. Beijing: Chemical Industry Press; 2018. p. 92.
[34] Zhou YH, Wang YX, Fan MZ. Incorporation of tyre rubber into wood plastic composites to develop novel multifunctional composites: Interface and bonding mechanisms. Ind Crops Prod. 2019;141:1–10.
[35] Wang H, Zhang M, He X, Du T, Wang Y, Li Y, et al. Facile prepared ball-like TiO_2 at GO composites for oxytetracycline removal under solar and visible lights. Water Res. 2019;160:197–205.
[36] Karbalaei-Bagher M, Ahmadi Z, Nazockdast H. A modus operandi toward interfacial enhancement of ethylene propylene diene monomer rubber/polybenzoxazine blends using EPDM-grafted-vinyltrimethoxysilane copolymer. Polym Eng Sci. 2021;61(3):810–21.
[37] Yang Z, Huang Y, Xiong YZ. A functional modified graphene oxide/nanodiamond/nano zinc oxide composite for excellent vulcanization properties of natural rubber. RSC Adv. 2020;10(68):41857–70.
[38] Zhang H, Yang H, Shentu B, Chen S, Chen M. Effect of titanium dioxide on the UV-C ageing behavior of silicone rubber. J Appl Polym Sci. 2018;135:1–14.
[39] Zou Y, He J, Tang Z, Zhu L, Liu F. Structural and mechanical properties of styrene–butadiene rubber/silica composites with an interface modified in-situ using a novel hindered phenol antioxidant and its samarium complex. Compos Sci Technol. 2020;188:107984.
[40] Wei Y-C, Liu G-X, Zhang H-F, Zhao F, Luo M-C, Liao S. Non-rubber components tuning mechanical properties of natural rubber from vulcanization kinetics. Polymer. 2019;183:121911.
[41] Gurbuz R, Sarac B, Soprunyuk V, Yuce E, Eckert J, Ozcan A, et al. Thermomechanical and structural characterization of polybutadiene/poly(ethylene oxide)/CNT stretchable electrospun fibrousmembranes. Polym Adv Technol. 2021;32(1):248–61.
[42] Guo Z, Huang CX, Chen Y. Experimental study on photocatalytic degradation efficiency of mixed crystal nano-TiO_2 concrete. Nanotechnol Rev. 2020;9(1):219–29.